AIAA 79-1731R

Combined Optimal/Classical Approach to Robust Missile Autopilot Design

F. William Nesline,* Brian H. Wells,† and Paul Zarchan‡
Raytheon Company, Bedford, Mass.

The direct application of optimal control techniques to a complete autopilot design leads to a control system that requires additional instrumentation and is sensitive to variations in the high-frequency model. A design approach is presented which utilizes classical control theory to bound the high-frequency design and modern control theory to obtain optimal low-frequency performance. Results are presented for a separation roll autopilot demonstrating the appropriate tradeoffs and benefits associated with the new design procedure.

Nomenclature

A = autopilot gain ratio
$\hat{a}, \hat{b}$ = performance index constant
a, b = scaled performance index constants
B = input control variable weighting matrix
B' = input matrix transposed
C = output state variable weighting matrix
c = performance index constant
D = input to output transmission matrix
F = system matrix
F' = system matrix transposed
F_1 = autopilot proportional gain
F_2 = autopilot integral gain
G_A = actuator transfer function
G_{FB} = flexible body transfer function
G_G = rate gyro transfer function
G_{RB} = rigid body transfer function
G_{NF} = notch filter transfer function
HG = total open-loop transfer function
J = performance index
$\hat{J}$ = scaled performance index
K_T = torsional mode gain
K = gain matrix solution of Riccati equations
K_δ = fin effectiveness
K_{FB} = flexible body gain constant
Q = performance index state variable weighting matrix
R = performance index control variable weighting matrix
s = complex variable
u = input control vector
u' = input vector transposed
x = state variable vector
x' = state variable vector transposed
y = output vector
δ = fin deflection
$\dot{\delta}$ = fin deflection rate
$\ddot{\delta}$ = fin deflection acceleration
δ_c = commanded fin deflection
$\delta_{c\max}$ = maximum commanded fin deflection
δ_P = pitch fin deflection
δ_R = roll fin deflection
δ_Y = yaw fin deflection
$\dot{\phi}$ = missile body roll rate
$\ddot{\phi}$ = missile body roll acceleration
$\dot{\phi}_M$ = measured missile body roll rate
$\ddot{\phi}_M$ = measured missile body roll acceleration
$\dddot{\phi}_M$ = measured missile body roll acceleration rate
$\dot{\hat{\phi}}$ = flexible body roll rate
$\ddot{\hat{\phi}}$ = flexible body roll acceleration
$\dot{\phi}_0$ = initial value of missile body roll rate
$\phi_{\max}$ = maximum allowable missile body angle
$\dot{\phi}_{\max}$ = maximum allowable missile body rate
ω_A = actuator bandwidth
ω_{CR} = total system open-loop crossover frequency
ω_D = notch filter denominator frequency
ω_G = rate gyro bandwidth
ω_N = notch filter numerator frequency
ω_{RR} = roll rate bandwidth
ω_Z = frequency of the combined rigid-body and torsional mode zero
ω_1 = torsional mode frequency
ζ_A = actuator damping ratio
ζ_G = gyro damping ratio
ζ_D = notch filter denominator damping ratio
ζ_N = notch filter numerator damping ratio
ζ_1 = torsional mode damping ratio

Presented as Paper 79-1731 at the AIAA Guidance and Control Conference, Boulder, Colo., Aug. 6-8, 1979; submitted Nov. 9, 1979; revision received July 14, 1980.

*Consulting Scientist, Guidance and Control, Missile Systems Division. Member AIAA.
†Engineer, Guidance and Control, Missile Systems Division.
‡Senior Engineer, System Design Laboratory, Missile Systems Division. Member AIAA.

Introduction

AIR-launched missiles require active autopilot control for safe separation from modern launch aircraft because 1) the flowfield in the vicinity of the aircraft causes large torque disturbances on the missile and 2) the aircraft may be maneuvering when it releases its missile. The effect of these disturbances and initial conditions are typically sensed by rate gyros and accelerometers whose outputs are connected through autopilot control circuitry to fin actuators.

Autopilot design is carried out initially by decoupling the pitch, yaw, and roll channels.[1] When this is done, classical control theory has proved itself to be a valuable and efficient tool for autopilot design. However, aerodynamic cross-coupling exists because the surface features of the missile create asymmetric flowfields over the control surfaces at different orientations of wind angle and angle of attack. A simplified block diagram showing the cross-coupling appears in Fig. 1. Here, if the roll rate response time is close enough to the pitch/yaw response time and the cross-coupling aerodynamic gain is high enough, instability can result. Therefore, successful autopilot design must take into consideration aerodynamic cross-coupling.

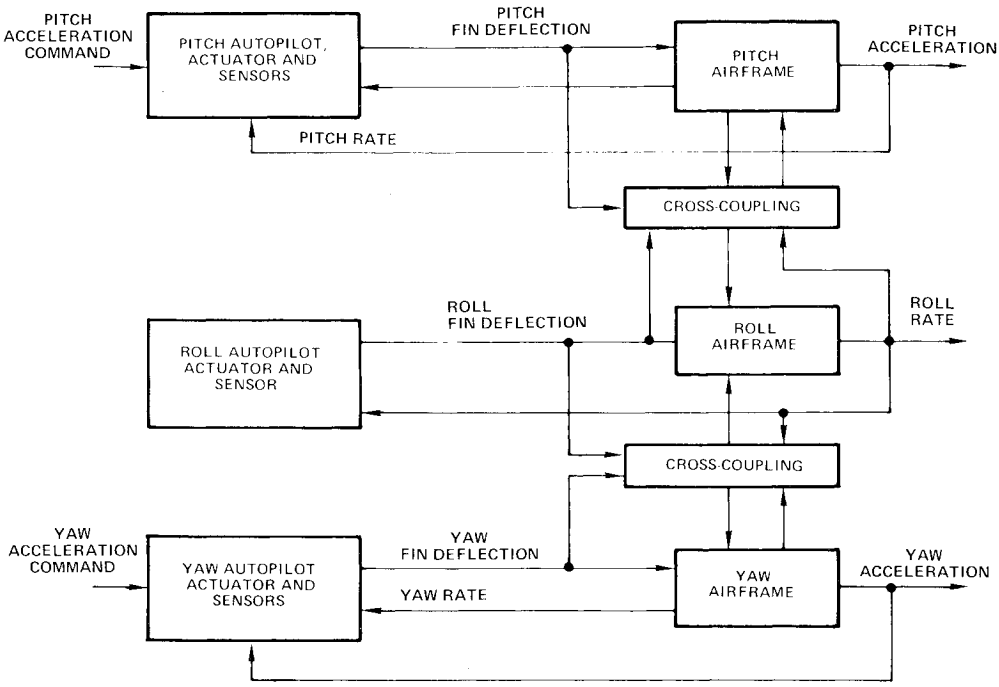

Fig. 1 Simplified block diagram showing cross-coupling.

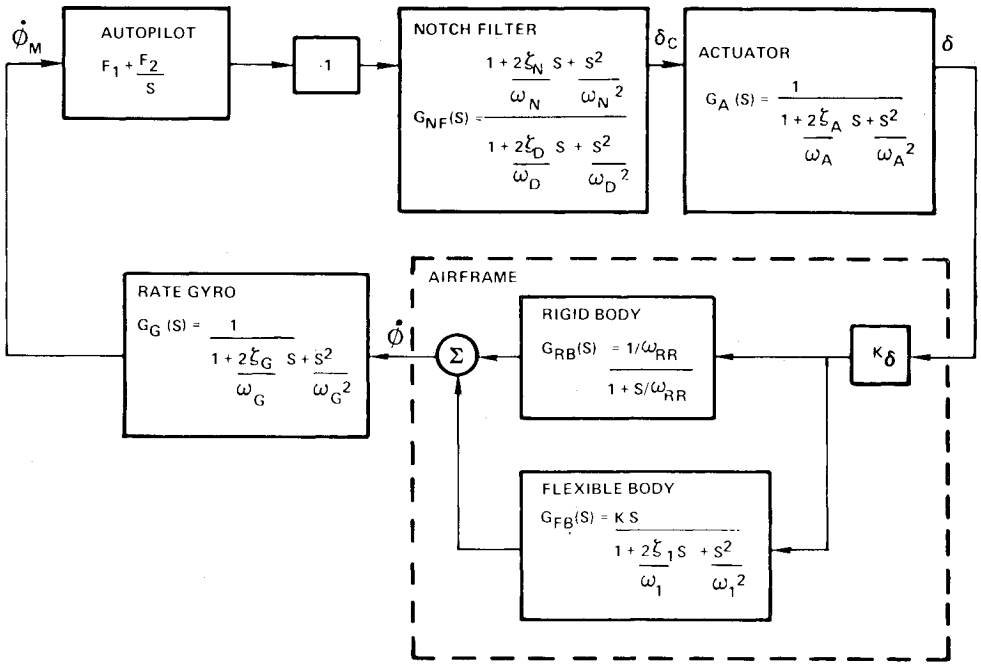

Fig. 2 Dynamic model for classical design approach.

Although classical design techniques are well established[2-6] and relatively straightforward for planar autopilot design, trial and error must be used when aerodynamic cross-coupling is considered. On the other hand, modern control theory[7,8] is well suited to the multiple input-output nature of the cross-coupled autopilot design. However, direct application of modern control theory to this problem, when high-frequency effects are considered, results in a design that requires additional instrumentation and is sensitive to variations in the high-frequency dynamic model. When high-frequency effects are neglected in the application of modern control theory, unacceptable, perhaps unstable, designs often result in the real system.[9]

The purpose of this paper is to show how modern control theory can be used in conjunction with classical control theory to achieve a robust design which deals with the uncertainties of the high-frequency effects while giving optimal performance in the low-frequency area. For simplicity, this approach will be presented for a separation roll autopilot to show the appropriate tradeoffs and benefits associated with the new design procedure. In order that this combined approach be fully understood, the classical and modern design approaches to this problem are reviewed.

Classical Design Approach

The classical design approach utilizes stability derivatives to derive transfer functions that describe the dynamic behavior of the airframe in the vicinity of the trim point. The transfer function which forms the basis of the roll autopilot design is

$$\frac{\dot{\phi}}{\delta}(s) = \frac{K_\delta}{\omega_{RR}}\left[\frac{1}{1+s/\omega_{RR}}\right] \tag{1}$$

Typically the roll rate response determined from Eq. (1) is too slow and must be made faster by the autopilot. The maximum roll angle and rate must be kept within limits to insure a safe and controlled launch. For these reasons, the roll autopilot is a proportional plus integral control.

The actuator bandwidth must be high for a fast-response homing missile and may be greater than 150 rad/s. In addition, since the rate gyro is mounted on a flexible missile, it senses torsional modes. The frequencies and dampings of these modes vary with temperature, the amount of fuel expended, the mass distribution of the missile parts, the number of sections, how the sections are joined, and the location of the rate gyro in the missile.

The classical design approach uses a high-order dynamic model for the actuator, missile aerodynamics, and rate gyro dynamics, including torsional effects. The autopilot is designed to achieve maximum crossover frequency given the actuator and rate gyro bandwidths and the first torsional mode.[1] If the first torsional mode limits the crossover frequency, or causes excessive peaking due to its low damping, the mode peak can be attenuated by using a notch filter.[10] The filter is designed so that the notch is at the center of the uncertainty band of the modal frequency and that its bandwidth is wide enough to give adequate attenuation over the entire band. Such a filter is suboptimal, but it is robust. The open-loop gain must be set high enough to provide adequate phase and gain margins. For each design, the maximum missile roll angle and rate is calculated and compared with the limits required for a safe and controlled launch. Trial and error leads to an acceptable design for a set of aerodynamic parameters K_δ and ω_{RR}.

A typical classical design approach is best illustrated by considering the dynamic model made up of quadratic transfer functions shown in Fig. 2. The open-loop transfer functions, $HG(s)$, can be written by inspection as

$$HG(s)=\frac{F_1 s+F_2}{s}G_{NF}G_A K_\delta (G_{RB}+G_{FB})G_G \tag{2}$$

Initially, the flexible body and notch filter dynamics are neglected, so the open-loop transfer function becomes

$$HG(s)\mid_{\text{no flex}}=\frac{F_2 K_\delta}{\omega_{RR}}\frac{(1+s/A)G_A G_G}{s(1+s/\omega_{RR})} \tag{3}$$

where $A=F_2/F_1$. If $\omega_{RR}<A<\omega_A<\omega_G$ the gain crossover frequency, ω_{CR}, must satisfy $A<\omega_{CR}<\omega_A$ to insure good relative stability (to cross 0 dB at a slope of -20 dB/dec). Crossover occurs when the magnitude of the open-loop transfer function is unity (0 dB).

$$HG(s)\mid_{\text{no flex}}\approx\frac{F_2 K_\delta \omega_{CR}/A}{\omega_{RR}\omega_{CR}\omega_{CR}/\omega_{RR}}=\frac{F_2 K_\delta}{A\omega_{CR}}=1 \tag{4}$$

Therefore the crossover frequency is calculated from

$$\omega_{CR}=F_2 K_\delta/A=F_1 K_\delta \tag{5}$$

Equation (5) indicates that the autopilot gain, F_1, determines the crossover frequency. The crossover frequency must be chosen to be high enough to insure a wide autopilot bandwidth, but low enough to prevent stability problems due to actuator and rate gyro dynamics. The autopilot gain ratio A is chosen to yield satisfactory phase margin. Since the transfer functions of the actuator and rate gyro are assumed to be

$$G_A(s)=\frac{1}{1+(2\zeta_A/\omega_A)s+s^2/\omega_A^2} \qquad \text{(actuator)} \tag{6}$$

$$G_G(s)=\frac{1}{1+(2\zeta_G/\omega_G)s+s^2/\omega_G^2} \qquad \text{(rate gyro)} \tag{7}$$

then the phase angle of the open-loop transfer function at the crossover frequency can be calculated from Eq. (3).

The influence of the first torsional mode on the open-loop transfer function can be seen by leaving out the notch filter in Eq. (2). The open-loop transfer function becomes

$$HG(s)\mid_{\text{no notch}}=\frac{F_2 K_\delta (1+s/A)(G_{RB}+G_{FB})G_A G_G}{s} \tag{8}$$

The rigid- and flexible-body dynamics are given by the transfer functions

$$G_{RB}(s)=\frac{1/\omega_{RR}}{1+s/\omega_{RR}} \qquad \text{(rigid-body)} \tag{9}$$

$$G_{FB}(s)=\frac{K_T s}{1+(2\zeta_1/\omega_1)s+s^2/\omega_1^2} \qquad \text{(flexible-body)} \tag{10}$$

Expansion of Eq. (8) yields

$$HG(s)\mid_{\text{no notch}}=\frac{F_2 K_\delta (1+s/A)G_A G_G}{\omega_{RR}s(1+s/\omega_{RR})}\times\left[\frac{1+s(K_T\omega_{RR}+2\zeta_1/\omega_1)+s^2(K_T+1/\omega_1^2)}{1+(2\zeta_1/\omega_1)s+s^2/\omega_1^2}\right] \tag{11}$$

The open-loop transfer function of Eq. (11) is identical to that of Eq. (3) except for the bracketed term. This term is made up of a "quadratic over a quadratic" transfer function. The damping of both quadratics is quite low, while the frequency of the numerator, ω_z, is much higher than the frequency of the denominator, ω_1, where ω_z is given by

$$\omega_z=(K_T+1/\omega_1^2)^{-1/2} \tag{12}$$

An open-loop Bode diagram can be constructed for Eq. (11). The low damping of first torsional mode causes peaking such that the gain is very close to 0 dB. If the phase angle is less than -180 deg at this frequency, instability can result. The peak of this torsional mode can be attenuated by the use of a notch filter. The transfer function of the notch filter is given by

$$G_{NF}(s)=\frac{1+(2\zeta_N/\omega_N)s+s^2/\omega_N^2}{1+(2\zeta_D/\omega_D)s+s^2/\omega_D^2} \qquad \text{(notch filter)} \tag{13}$$

If the notch filter happens to be tuned to the torsional mode, then

$$\omega_N=\omega_D\approx\omega_1 \qquad \zeta_N\approx\zeta_1 \qquad \zeta_D=0.5 \tag{14}$$

Thus the damping of this mode ζ_1 will effectively be increased to ζ_D, yielding an open-loop transfer function

$$HG(s)=\frac{F_2 K_\delta}{\omega_{RR}}\frac{(1+s/A)G_A G_G}{s(1+s/\omega_{RR})}\times\left[\frac{1+s(K_T\omega_{RR}+2\zeta_1/\omega_1)+s^2(K_T+1/\omega_1^2)}{1+(2\zeta_D/\omega_D)s+s^2/\omega_D^2}\right] \tag{15}$$

Finally, a numerical example is presented in order to illustrate the various concepts used in a classical design. Nominal values for the airframe and sensor parameters are presented in Table 1. A notch filter is included in this example because the damping of the torsional mode is low ($\zeta_1=0.01$) and the mode peak must be attenuated. The autopilot gains F_1 and F_2 are to be selected so that a high crossover frequency resulting in adequate phase and gain margins will be achieved.

Using the values of Table 1, the phase margin can be calculated. The phase margin is displayed as a function of the

autopilot gain ratio A for different crossover frequencies in Fig. 3. Here it can be seen that increasing the autopilot gain ratio or the crossover frequency decreases the phase margin. In this example, a phase margin of 38 deg will be a design goal because the phase contributions of the torsional mode and notch filtering were not included in the calculation of phase margin. For this design goal, Fig. 3 indicates three possible solutions—$\omega_{CR}=45$, $A=2$; $\omega_{CR}=30$, $A=11$; or $\omega_{CR}=15$, $A=11$.

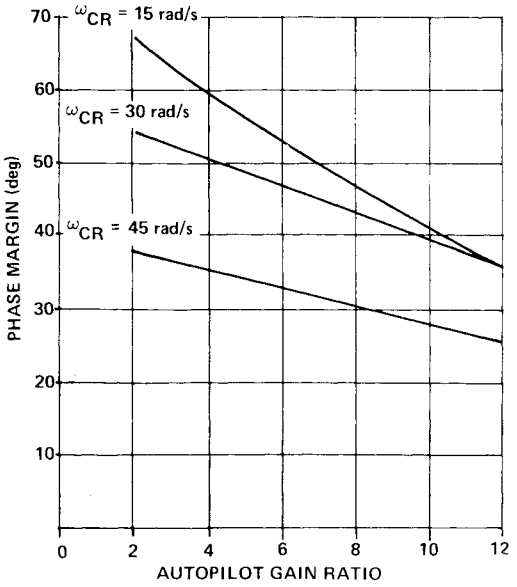

Fig. 3 Phase margin decreases with increasing autopilot gain ratio and crossover frequency.

The best solution is picked from the roll rate, roll angle, and fin deflection transient responses. Although the roll rate response is fastest for the highest crossover frequency, the roll angle transient response behaves in just the opposite way. Although the fin deflection response is fastest for the highest crossover frequency, the peak values also increase with crossover frequencies. For these reasons the nominal design is chosen to be $\omega_{CR}=30$, $A=11$. This design results in the autopilot gains:

$$F_1=\omega_{CR}/K_\delta=0.0033 \qquad F_2=AF_1=0.0367 \qquad (16)$$

The open-loop Bode plot utilizing this autopilot design appears in Fig. 4. Here it can be seen that the achieved phase margin is 32 deg while the gain margin is 5.3 dB.

For the example considered, the classical approach results in a design with good relative stability characteristics despite

Table 1 Nominal inputs

Name	Definition	Value
ω_{RR}	Roll rate bandwidth	2 rad/s
K_δ	Fin effectiveness	9000 $1/s^2$
ω_A	Actuator bandwidth	100 rad/s
ζ_A	Actuator damping	0.65
ω_G	Rate gyro bandwidth	200 rad/s
ζ_G	Rate gyro damping	0.5
ω_1	Torsional mode frequency	250 rad/s
ζ_1	Torsional mode damping	0.01
K_T	Torsional mode gain	−0.0000129
ω_N	Notch filter numerator frequency	250 rad/s
ζ_N	Notch filter numerator damping	0.01
ω_D	Notch filter denominator frequency	250 rad/s
ζ_D	Notch filter denominator damping	0.5

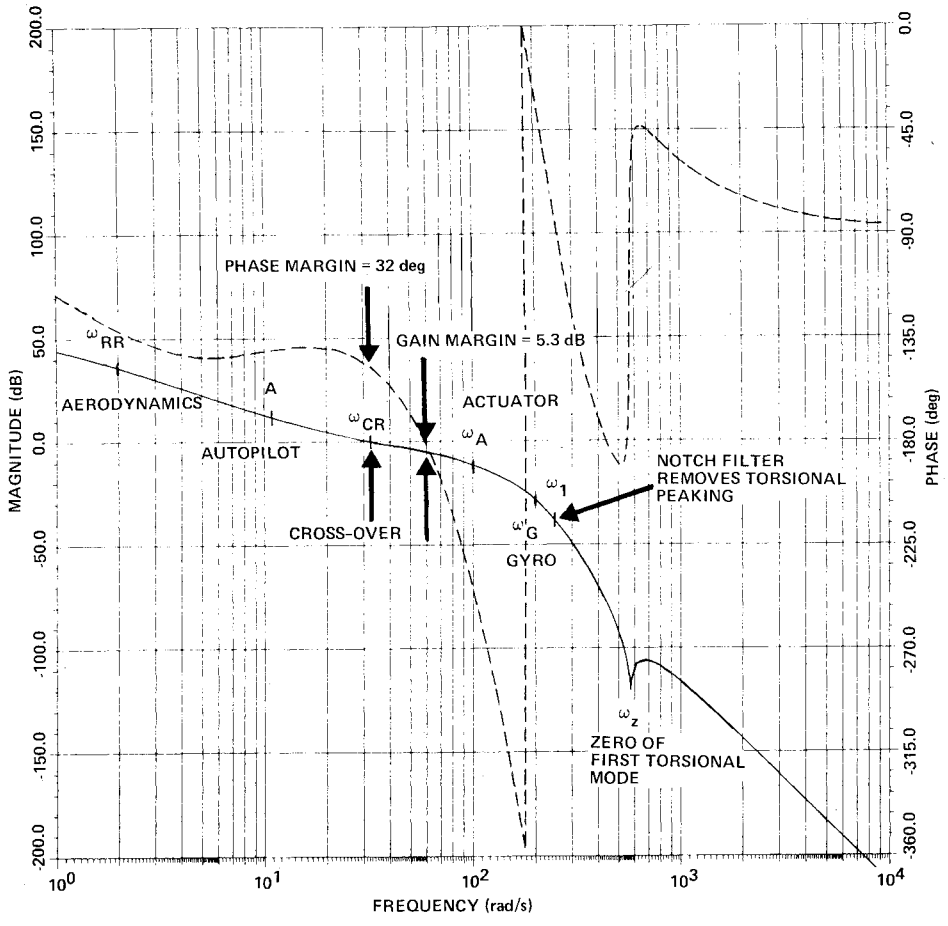

Fig. 4 Bode diagram of final design.

variations in the high-frequency dynamics of the airframe. While the classical approach is relatively straightforward for the planar design of the separation roll autopilot, it increases substantially in complexity for the full three-dimensional system, including aerodynamic cross-coupling.

Modern Control Design Technique

Modern control techniques produce an optimal linear regulator designed to keep the system at a desired reference condition.

The system is defined by

$$\dot{x}=Fx+Bu \qquad y=Cx+Du \tag{17}$$

where x is the state vector, u is the control vector, and y is the output vector. For the case being considered we will use state feedback, as the right half of Eq. (17) is not necessary.

The linear regulator is designed to minimize the quadratic performance index

$$J=\frac{1}{2}\int_0^\infty [x'Qx+u'Ru]\,dt \tag{18}$$

This gives the control law

$$u=-R^{-1}B'Kx \tag{19}$$

where K is the solution to the algebraic matrix Riccati equation,

$$KF+F'K-KBR^{-1}B'K+Q=0 \tag{20}$$

The designer chooses the matrices Q and R to be positive definite. Then the matrix Riccati equation is solved for K and finally the feedback matrix is calculated. The regulator will produce a stable system provided (F,B) is a controllable pair.

Optimal Design Using High-Frequency Effects

The system including high-frequency effects is shown in Fig. 2. A seventh-order model is needed to describe the complete dynamics. The model includes a quadratic actuator, rate gyro, and the first torsional mode along with a first-order model of the rigid-body airframe dynamics.

The controller will use the roll angle ϕ, which cannot be directly measured. This value is simply the integral of the roll rate $\dot{\phi}$. It is calculated by integrating the output of the gyro, $\dot{\phi}_m$, to obtain the estimated roll angle, ϕ_m. The system equations are augmented to include this additional state before the design is carried out. The eighth-order augmented system equations are:

$$\begin{bmatrix} \dot{\phi}_m \\ \ddot{\phi}_m \\ \dddot{\phi}_m \\ \ddot{\phi} \\ \dddot{\phi} \\ \ddot{\hat{\phi}} \\ \dot{\hat{\phi}} \\ \dot{\delta} \\ \ddot{\delta} \end{bmatrix} = \begin{bmatrix} 0 & 1 & 0 & 0 & 0 & 0 & 0 & 0 \\ 0 & 0 & 1 & 0 & 0 & 0 & 0 & 0 \\ 0 & -\omega_G^2 & -2\zeta_G\omega_G & \omega_G^2 & K_T\omega_G^2 & 0 & 0 & 0 \\ 0 & 0 & 0 & -\omega_{RR} & 0 & 0 & K_\delta & 0 \\ 0 & 0 & 0 & 0 & -2\zeta_1\omega_1 & -\omega_1^2 & K_\delta\omega_1^2 & 0 \\ 0 & 0 & 0 & 0 & 1 & 0 & 0 & 0 \\ 0 & 0 & 0 & 0 & 0 & 0 & 0 & 1 \\ 0 & 0 & 0 & 0 & 0 & 0 & -\omega_A^2 & -2\zeta_A\omega_A \end{bmatrix} \begin{bmatrix} \phi_m \\ \dot{\phi}_m \\ \ddot{\phi}_m \\ \dot{\phi} \\ \ddot{\phi} \\ \dot{\hat{\phi}} \\ \hat{\phi} \\ \delta \\ \dot{\delta} \end{bmatrix} + \begin{bmatrix} 0 \\ 0 \\ 0 \\ 0 \\ 0 \\ 0 \\ 0 \\ 0 \\ \omega_A^2 \end{bmatrix} \delta_C \tag{21}$$

$$\underbrace{\dot{X}}_{} = \underbrace{F}_{} \underbrace{X}_{} + \underbrace{B}_{}$$

The performance index is given by Eq. (18) where Q is 8×8 and positive definite and R is a scalar (>0). The matrix Riccati equation for the full system is a system of eight nonlinear equations.

The direct implementation of the feedback controller requires measurements or estimates of all eight states. In a homing missile, sensors would have to be added to provide the necessary measurements, but the added weight, cost, complexity, and reduced reliability make this alternative unattractive. The unmeasured states can be estimated using observers. However, the large data base required to properly represent the system dynamics at the high frequencies over the whole flight envelope adds substantial complexity to the system. At present, the large computer throughput required for the implementation of the necessary observers is not feasible for an on-board missile computer. Therefore, it is inappropriate in this application to consider optimal design using a complete low- and high-frequency model.

Optimal Design Using a Low-Frequency Model

The model used for design must be simplified to make the modern control approach more feasible. To minimize the perturbations in the roll rate $\dot{\phi}$ due to disturbances, these must be present in the simplified model. The dynamic frequencies of $\dot{\phi}$ and ϕ are low compared to the frequency dynamics of the actuator, gyro, and the first torsional mode. The intermediate states of the actuator and the gyro cannot be easily measured and the knowledge of the characteristics (damping ratio and natural frequency) of the first torsional mode are uncertain. For these reasons, the actuator, gyro, and structural resonance will be excluded from the simplified model. The actuator and gyro will be modeled as ideal (transfer functions = unity gain). The torsional mode will be ignored at present but will be added after the low-frequency design is complete.

The simplified model describing the low-frequency dynamics of the system is

$$\ddot{\phi}=-\omega_{RR}\cdot\dot{\phi}+K_\delta\cdot\delta_c \qquad \dot{\phi}(0)=\dot{\phi}_0 \tag{22}$$

where the parameters were defined in the previous section.

The augmented system is created by adding an integrator to obtain the roll angle from the roll rate. This gives us

$$\ddot{\phi}=-\omega_{RR}\cdot\dot{\phi}+K_\delta\cdot\delta_c \qquad \dot{\phi}=\dot{\phi} \tag{23}$$

which is shown in Fig. 5. The performance index is

$$J=\frac{1}{2}\int_0^\infty \begin{bmatrix} \dot{\phi} \\ \phi \end{bmatrix}' Q \begin{bmatrix} \dot{\phi} \\ \phi \end{bmatrix} + \delta_c^2 R\,dt \tag{24}$$

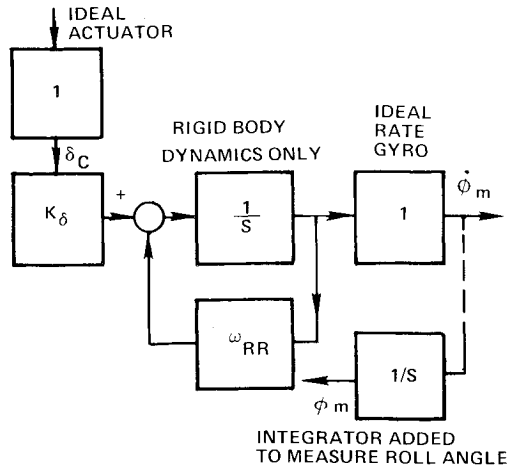

Fig. 5 Augmented simplified system model.

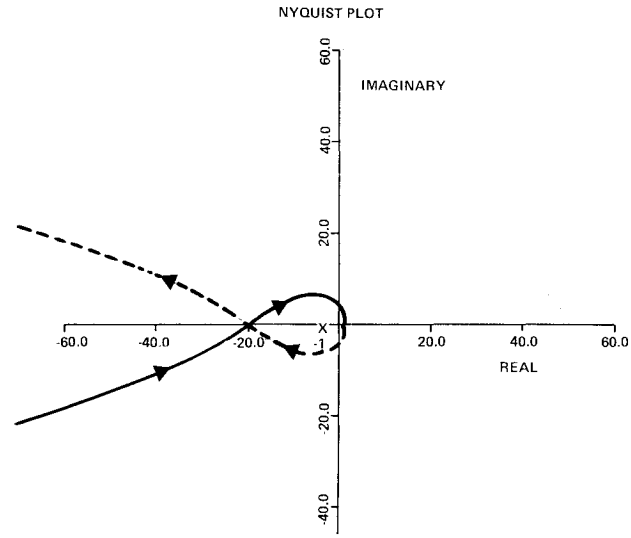

Fig. 6 Encirclement of the −1.0 point shows that the design values create an unstable system.

where the performance index matrices are chosen to be

$$Q=\begin{bmatrix} a & 0 \\ 0 & b \end{bmatrix} \tag{25}$$

and $R=c$. The performance index can be scaled without changing the design, thus giving

$$\hat{J}=\int_0^\infty (\hat{a}\dot{\phi}^2+\hat{b}\phi^2+\delta_c^2)\,dt \tag{26}$$

where

$$\hat{a}=a/c \qquad \hat{b}=b/c \qquad \hat{J}=2\cdot J \tag{27}$$

The feedback control law from Eq. (19) is

$$\delta_c=-F_1\dot{\phi}-F_2\phi \tag{28}$$

where F_1 and F_2 are found by solving

$$F_1^2+2\omega_{RR}/K_\delta\cdot F_1-(2/K_\delta)F_2-\hat{a}=0 \tag{29}$$

and

$$F_2^2-\hat{b}=0 \tag{30}$$

which came from the algebraic matrix Riccati equation (20).

The simplified augmented system yields a proportional plus integral controller which is the same form as the controller obtained using the classical design method. The gains are a function of two performance index parameters which are directly related to physical quantities, the roll rate, and the roll angle.

The performance index parameters are chosen by examining the time responses of $\dot{\phi}$ and ϕ for different values of $\hat{a}$ and $\hat{b}$. As a first guess, use[8]

$$J=\frac{1}{2}\int_0^\infty\left(\frac{\dot{\phi}^2}{\dot{\phi}^2_{\max}}+\frac{\phi^2}{\phi^2_{\max}}+\frac{\delta_c^2}{\delta^2_{c\,\max}}\right)dt \tag{31}$$

as a performance index where $\dot{\phi}_{\max}$ is the maximum desired value of $\dot{\phi}$ (300 deg/s), $\phi_{\max}$ is the maximum desired value of ϕ (10 deg), and $\delta_{c\max}$ is the maximum available value of δ_c (30 deg). These give

$$\hat{a}=\delta^2_{c\max}/\phi^2_{\max}=0.01\,s^2 \qquad \hat{b}=\delta^2_{c\max}/\phi^2_{\max}=9 \tag{32}$$

for the performance index parameters which yield feedback gains of $F_1=0.103$ and $F_2=3.0$.

These gains were used in the full-system model, which includes high-frequency dynamics. Figure 6 shows the Nyquist plot for the full system. From this it can be seen that the full system is unstable, although the simplified system is stable and yields excellent responses.

The modern control design applied to the full system will yield a stable system provided that the following conditions are met: 1) Q and R are positive definite, and 2) (F,B) represent a controllable pair.

However, when the system is simplified, the controller obtained will not produce a stable system for all positive define choices of Q and R even though the new (F,B) pair is still controllable.

The optimal design using the simplified model ignores the stability constraints imposed on the high-frequency dynamics that were removed to make the model simpler. Additional constraints are required to insure that the design using the simplified model will produce a stable system.

Combined Optimal/Classical Design

A combined optimal/classical approach can be used to avoid an unstable system design. The simplified model of the system is used for the optimal design with the classical design techniques supplying the additional constraints.

For the simplified optimal design, the actuator and gyro are modeled as ideal, while the first torsional mode is ignored. The classical methods are used to design a notch filter that eliminates stability problems caused by the first torsional mode, as discussed in the section on the classical design techniques. A reasonable value of crossover frequency is then chosen which reduces the number of free performance index parameters from two to one.

In the simplified optimal design, two performance index parameters ($\hat{a}$ and $\hat{b}$) had to be specified to determine the autopilot gains (F_1 and F_2). Provided that $F_2/F_1<K_\delta\cdot F_1$, it can be shown that

$$\omega_{CR}=K_\delta\cdot F_1 \tag{33}$$

Thus, by choosing ω_{CR} the value for F_1 has been specified. Now the gain, Eqs. (29) and (30), can be solved by choosing $\hat{a}$ *or* $\hat{b}$. The condition that $F_2/F_1<K_\delta\cdot F_1$ is always met because it is a necessary condition for the simplified system to be stable, and the optimal design yields a stable system, provided the high-frequency dynamics are not included. Specifying either one of the performance index parameters sets the values of F_2 and the other performance index parameter. Values of $\hat{a}$

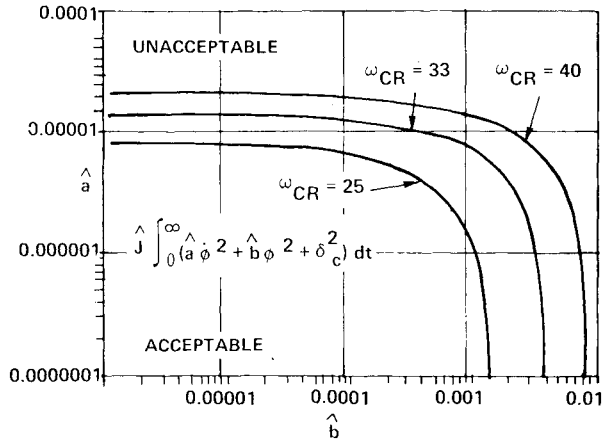

Fig. 7 Lines of constant crossover frequency.

can be plotted vs $\hat{b}$ with ω_{CR} constant. The lines of constant crossover frequency can be used to divide the performance index plane into acceptable and unacceptable regions. Figure 7 shows the constant ω_{CR} lines. The lower left side will be the acceptable region, while the upper right is unacceptable.

The combined optimal/classical design consists of four basic steps. First, the full system is simplified. The low-frequency states and the states whose performance will be measured are used to make the simplified system. Second, the optimal design is used on the simplified system to find the gains as a function of the performance index. Third, classical design methods are used to provide additional constraints, such as crossover frequency, for the simplified optimal design. The classical design techniques may also be used to remove some of the unwanted high-frequency effects that cause stability problems. Finally, the additional constraints are used to bound the performance index parameters, thus creating a set of acceptable parameter values and a set of unacceptable parameter values. The result is an optimal low-frequency system that has good relative stability despite high-frequency effects.

The numerical example presented for the classical design is repeated using the combined optimal/classical design method. Table 1 contains the nominal values of the airframe and sensor parameters. The notch filter is designed using classical techniques. The classical techniques also specify a crossover frequency.

The crossover frequency is selected by examining the high-frequency portion of the Bode plot for the system. The controller introduces only minor changes to the high-frequency portion of the system, thus the crossover frequency can be selected without completely specifying the controller. The crossover should occur at a point where the Bode plot has a -20 dB/dec slope and far enough away from frequency breaks to minimize their effects. The first break point in the high-frequency portion of the Bode plot is caused by the actuator at 100 rad/s. After this point, the Bode plot drops off at -60 dB/dec. A good rule of thumb is to make the crossover frequency one third of the frequency of this first breakpoint. For this case, a crossover frequency of 33 rad/sec is chosen. This set the value of F_1 at $33/9000 = 0.0037$.

Now, specifyinga value for $\ddot{a}$ or $\ddot{b}$ will complete the design. For this case, a ratio of the two gains will be chosen instead. The ratio of relative importance of the roll rate as compared to the roll angle $(\hat{a}/\hat{b})$ is chosen as the ratio of the squares of the maximum desired values of each. This ratio $\dot{\phi}^2_{\max}/\phi^2_{\max}$ is approximately 1000. Transient responses show this to be a reasonable ratio. Using the ratio between $\hat{a}$ and $\hat{b}$ and the value of F_1 determined from the crossover frequency, F_2 is found to be 0.053. This gives an autopilot gain ratio of 14.7.

The controller developed using the combined optimal/classical design method on the simplified system model produces a controller that has good relative stability. The performance of the system and the final design values are comparable to those resulting from the classical design, this verifying the method.

Conclusions

A combined optimal/classical design approach for air-launched missile separation autopilots has the advantages of both methods and eliminates the major disadvantages of each method alone. The combined method allows a practical design by using optimal design techniques on a simplified low-frequency system model that contains constraints from the high-frequency dynamics. The procedure reduces the instrumentation and the design problems that result from an optimal design that requires the full-frequency system model. At the same time, the new procedure gives the advantages of modern matrix analysis for coupled systems. The resulting system has good relative stability despite variation in the high-frequency dynamics of the missile airframe. In the separation roll autopilot example shown, the classical design techniques were used to establish an acceptable crossover frequency, which was chosen to give good relative stability. This was then used to add an extra constraint to the optimal design, which was carried out with a simplified model of the system that contained only low-frequency dynamics. Results show the design yields a fast responding, stable system that is robust to high-frequency parameter variations.

References

[1] Nesline, F.W. and Nabbefeld, N.C., "Design of Digital Autopilots for Homing Missiles," presented at the AGARD Flight Mechanics Panel Symposium, London, England, May 21-24, 1979.

[2] Bode, H.W., *Network Analysis and Feedback Amplifier Design,* D. Van Nostrand Company, Inc., Toronto, 1945, pp. 170-275.

[3] Nyquist, H., "Regeneration Theory," *Bell System Technical Journal,* Vol. 11, 1932, pp. 126-247.

[4] Hall, A.C., *The Analysis and Synthesis of Linear Servomechanisms,* MIT Press, Cambridge, Mass., 1943, pp. 121-189.

[5] Oldenburger, R., *Frequency Response,* MacMillan, New York, 1956, pp. 157-236.

[6] MacFarlane, A.G.J. (ed.), *Frequency-Response Methods in Control Systems,* IEEE Press, New York, 1979, pp. 17-138.

[7] Athans, M. and Falb, P.L., *Optimal Control. An Introduction to the Theory and Its Applications,* McGraw-Hill, New York, 1966, pp. 364-508.

[8] Bryson, A.E. and Ho, Y., *Applied Optimal Control,* Blaisdell Publishing Company, Waltham, Mass., 1969, pp. 148-176.

[9] Gupta, N.K., "Frequency-Shaped Cost Functionals: An Extension of Linear-Quadratic-Gaussian Design Methods," *Journal of Guidance and Control,* Vol. 3, Nov.-Dec. 1980, pp. 529-535.

[10] Andeen, R.E., "Stabilizing Flexible Vehicles," *Astronautics & Aeronautics,* Vol. 2, Aug. 1964, pp. 38-44.